One-Dimensional Mathematical Model of the Atrioventricular Node Including Atrio-Nodal, Nodal, and Nodal-His Cells

S. Inada,[†] J. C. Hancox,[‡] H. Zhang,[†] and M. R. Boyett[†*]
[†]University of Manchester, Manchester, United Kingdom; and [‡]University of Bristol, Bristol, United Kingdom

ABSTRACT Mathematical models are a repository of knowledge as well as research and teaching tools. Although action potential models have been developed for most regions of the heart, there is no model for the atrioventricular node (AVN). We have developed action potential models for single atrio-nodal, nodal, and nodal-His cells. The models have the same action potential shapes and refractoriness as observed in experiments. Using these models, together with models for the sinoatrial node (SAN) and atrial muscle, we have developed a one-dimensional (1D) multicellular model including the SAN and AVN. The multicellular model has slow and fast pathways into the AVN and using it we have analyzed the rich behavior of the AVN. Under normal conditions, action potentials were initiated in the SAN center and then propagated through the atrium and AVN. The relationship between the AVN conduction time and the timing of a premature stimulus (conduction curve) is consistent with experimental data. After premature stimulation, atrioventricular nodal reentry could occur. After slow pathway ablation or block of the L-type Ca^{2+} current, atrioventricular nodal reentry was abolished. During atrial fibrillation, the AVN limited the number of action potentials transmitted to the ventricle. In the absence of SAN pacemaking, the inferior nodal extension acted as the pacemaker. In conclusion, we have developed what we believe is the first detailed mathematical model of the AVN and it shows the typical physiological and pathophysiological characteristics of the tissue. The model can be used as a tool to analyze the complex structure and behavior of the AVN.

INTRODUCTION

The atrioventricular node (AVN) lies between the atria and the ventricles and is the only site where the action potential can pass between the two sets of chambers. Slow conduction of the action potential through the AVN facilitates efficient pumping of blood by creating a delay between atrial and ventricular systole. Slow atrioventricular (AV) conduction is also important during arrhythmias such as atrial fibrillation (AF) by limiting the number of action potentials transmitted to the ventricle. The AVN is frequently the site of reentrant rhythms; the slow and fast pathways into the AVN are believed to be the substrate for AV nodal reentry. In addition, the AVN acts as a subsidiary pacemaker and controls ventricular rate when the sinoatrial node (SAN) fails. The electrophysiological behavior of the AVN is, therefore, rich, complex and important (1,2).

Action potential models based on experimental data are repositories of knowledge as well as important research and teaching tools to analyze complex phenomena such as arrhythmias. There are many action potential models for the SAN, atrial muscle, Purkinje fibers, and ventricular muscle, but not for the AVN (3). Liu et al. (4) developed a Hodgkin-Huxley type action potential model for the rabbit AVN. However, additional experimental data have become available since the model was published and the model did not allow for the heterogeneity of the AVN (5). De Carvalho and De Almeida (6) classified the AVN into three regions based on action potential shapes: the AN (atrio-nodal), N (nodal), and NH (nodal-His) regions. The differences in action potential shape among these three regions are likely to be the result of differences in ionic currents (5,7,8). In this study, we developed a family of biophysically detailed AVN action potential models for the AN, N, and NH regions, and analyzed the characteristics of the AVN including dual pathway conduction, AV nodal reentry, and its filtering function.

METHODS

At the AV junction, a tract of nodal tissue connects the atria and ventricles. Part of the tract (penetrating bundle) is enclosed in connective tissue as it passes through the fibrous annulus separating the atria and ventricles. There are two inputs into the penetrating bundle, the slow and fast pathways. The slow pathway corresponds to the inferior nodal extension (running just above tricuspid valve from coronary sinus to penetrating bundle). We assume the slow pathway is made up of N cells (9–11). The fast pathway is more superior and is thought to be made up of transitional AN cells (9). The compact node, present at the start of the penetrating bundle, is common to the slow and fast pathways and is also thought to be made up of N cells (11). We assume the bulk of the penetrating bundle is made up of NH cells (9). Models of the action potentials of AN, N, and NH cells in the rabbit were developed as described in the Supporting Material.

A simplified one-dimensional (1D) multicellular model (string of cells) for the SAN, right atrium and AVN of the rabbit was developed. The string of cells representing the SAN included both central and peripheral cells. The action potentials in rabbit central and peripheral SAN cells were calculated using the models of Zhang et al. (12). The action potential in rabbit atrial cells was calculated using a modified version of the model of Lindblad et al. (13). Action potentials in rabbit AN, N, and NH cells were calculated using the models described in the Supporting Material. Neighboring cells were coupled by a coupling conductance, g_j. The coupling conductance was varied to give appropriate conduction times and velocities. However, the final coupling conductances are consistent with what is known of the

Submitted February 27, 2009, and accepted for publication June 30, 2009.

*Correspondence: mark.boyett@manchester.ac.uk

Editor: Michael D. Stern.

0006-3495/09/10/2117/11 $2.00

doi: 10.1016/j.bpj.2009.06.056

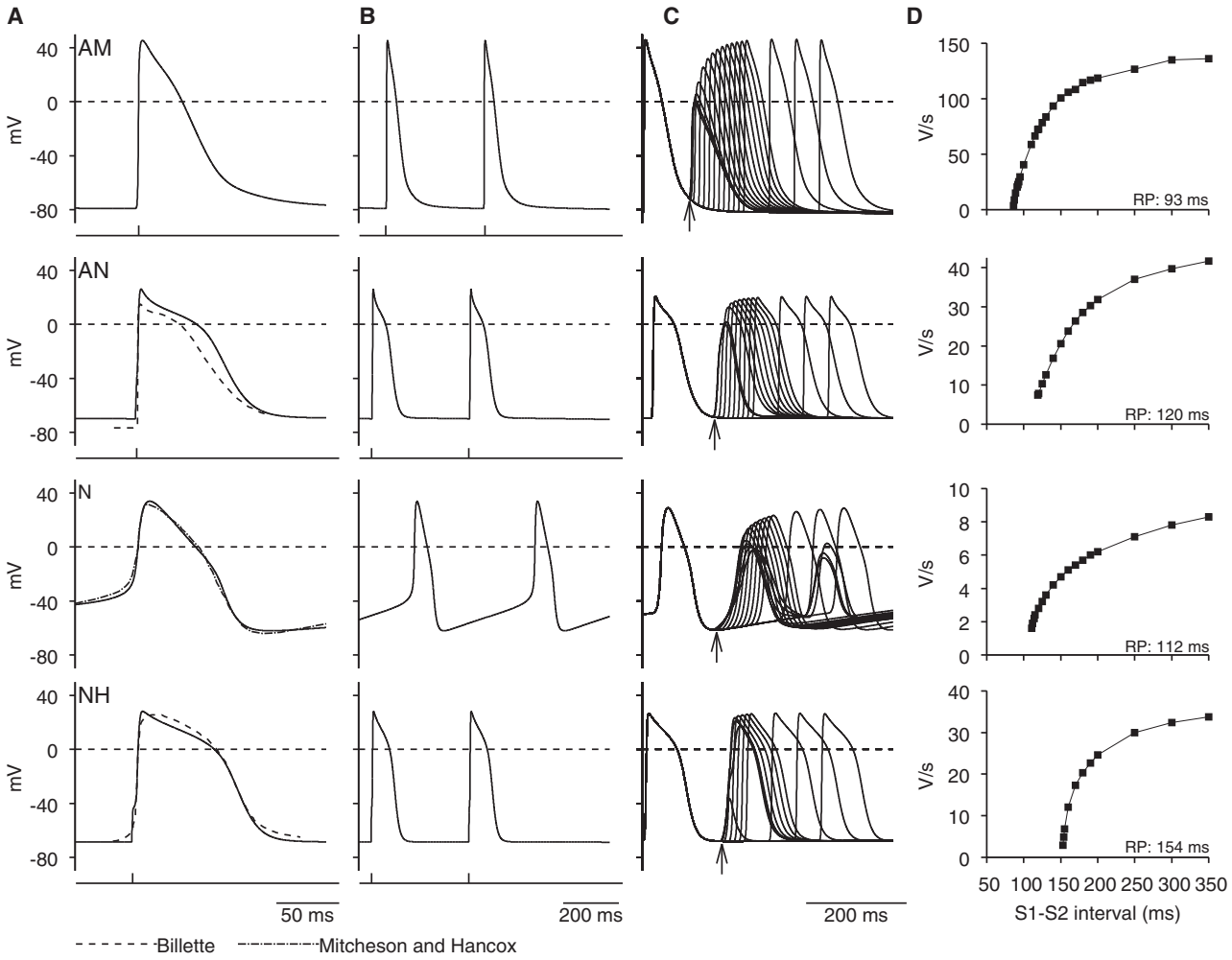

FIGURE 1 Computed action potentials in atrial (AM), AN, N, and NH cells. (*A* and *B*) Computed action potentials (*solid lines*) at (*A*) fast and (*B*) slow time bases. With one exception (N cell action potentials are spontaneous), action potentials were triggered by stimulus (1 ms; 1.2 × threshold); stimuli are shown below action potentials. Experimentally recorded AN, N, and NH action potentials are also shown in *A* (*dashed line* (9); *dashed-dotted line* (35)). (*C*) Measurement of restitution. In four models, premature action potentials (in response to S2 stimulus) were triggered at different intervals after control action potential (in response to S1 stimulus). Control and premature action potentials from different runs are superimposed. Stimuli (1 ms in duration): 1.2 × threshold for AN and NH cells; 2.0 × threshold for N cells. Basic stimulus interval, 350 ms (2.9 Hz). Arrows highlight refractory period. (*D*) Restitution curves. Curves show relationship between dV/dt_{max} and S1-S2 interval; refractory period (RP) shown. For *A* and *B*, single cell models were used. However, for *C* and *D*, 1D multicellular model shown in Fig. 5 *A* was used to ensure that premature action potentials were capable of propagation; one end of string was stimulated and action potentials were recorded from middle of string of relevant cells.

electrical coupling and expression of connexins (responsible for gap junctions and electrical coupling) in the different regions. For further details see the Supporting Material.

RESULTS

Action potentials of atrial, AN, N, and NH cell models

The solid lines in Fig. 1 *A* show action potentials generated using the atrial, N, AN, and NH models at a fast time base. The model traces are superimposed on action potentials recorded experimentally from the different cell types (Fig. 1 *A*, *dashed lines* and *dashed-dotted line*). Only the N cell model has automaticity—the N cell action potentials shown are spontaneous, whereas the remainder are triggered. The model action potentials are a reasonable fit to the experimental ones. Fig. 1 *B* shows action potentials generated using the different models at a slow time base. Fig. 1 *C* shows premature model action potentials triggered at different intervals (S1-S2) after a steady-state response (basic stimulation interval, 350 ms). In Fig. 1 *D*, dV/dt_{max} of the premature action potential is plotted against the S1-S2 interval. dV/dt_{max} was high at long S1-S2 intervals and decreased as the S1-S2 interval was decreased; when the refractory period was reached, the premature action potential failed. In atrial, AN, N, and NH cells, the refractory periods are 93, 120, 112, and 154 ms, respectively, similar to the refractory periods in the rabbit measured experimentally

TABLE 1 Refractory periods in simulation and experiment

		Experiment		
	Simulation	J. Billette (unpublished data)	Reid et al. (25)	Lin et al. (26)
Atrial cell	93	81 ± 5	—	—
AN cell/fast pathway	120	127 ± 9*	141 ± 15*	—
N cell /slow pathway	112	91 ± 12	91 ± 10	100 ± 9
NH cell	154	—	—	—

In simulations, the refractory periods were calculated using the 1D multicellular model shown in Fig. 5 *A* (see Fig. 1 for details).
*Value obtained after slow pathway ablation.

(Table 1). Action potential characteristics in simulation and experiment are compared in Fig. 2; the two are comparable.

1D multicellular model of AVN

A simplified 1D multicellular model (string of cells) for the SAN, right atrium, and the AVN of the rabbit was developed. Fig. 3 *A* shows a schematic diagram of the multicellular model and Fig. 3 *B* shows how it relates to the anatomy. In the configuration shown in Fig. 3 *A*, it consisted of a string of 25 SAN cells (central and peripheral SAN cells) connected to a string of 75 atrial cells. The atrial cells were connected to two parallel pathways, the slow pathway (string of 75 atrial cells and 125 N cells) and the fast pathway (string of 50 atrial cells, 75 AN cells, and 25 N cells). Finally, both pathways were connected to a common string of 25 N cells and 75 NH cells. Neighboring cells were coupled by a coupling conductance. Fig. 3 *C* shows how the cell capacitance (C_m), coupling conductance (g_j) and the Na^+ conductance (g_{Na}) governing I_{Na} vary along the length of the multicellular model.

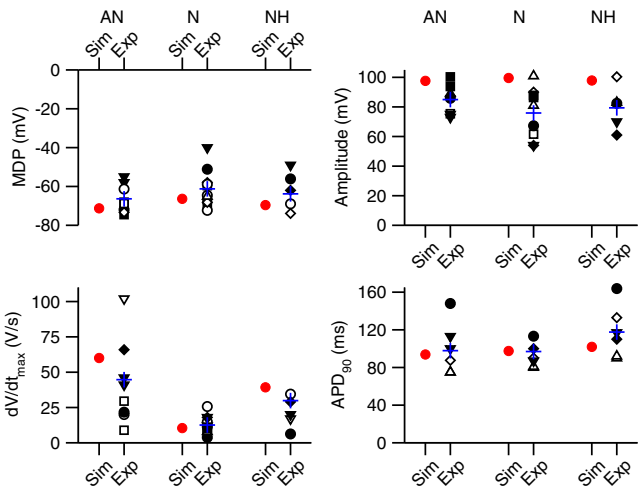

FIGURE 2 Comparison of action potential characteristics. Maximum diastolic potential (MDP), maximum upstroke velocity of the action potential (dV/dt_{max}), action potential amplitude and action potential duration at 90% repolarization (APD_{90}) in AN, N, and NH cells in simulations (Sim; *red* or *gray symbols*) and experiments (Exp; *black symbols*) shown. □ (36); ○ (37); △ (38); ▽ (9); ◇ (39); ■ (40); • (7); ▲ (41); ▼ (42); ◆ (24). Blue or gray cross, mean of experimental data.

Action potential propagation from SAN through atrium to AVN

Fig. 4 shows the result of a simulation using the 1D multicellular model shown in Fig. 3 *A*. Fig. 4 *A* shows selected action potentials (and dV/dt) from the center and periphery of the SAN, atrial muscle, and AN, N, and NH cells. Fig. 4 *B* shows many more action potentials along the string of tissue. Activation times, i.e., times taken for the action potential to propagate from the center of the SAN to specific points, were measured (recording point, −30 mV during action potential upstroke). Fig. 4 *C* shows the activation time at selected points along the pathway: center of the SAN (point *a*); periphery of the SAN (point *b*), atrial muscle at the starting point of the fast and slow pathways (point *c*), middle of the fast and slow pathways, proximal penetrating bundle (point *d*) and bundle of His (i.e., distal penetrating bundle; point *e*). Fig. 4, *A–C*, shows that the action potential was first initiated in the center of the SAN. It then propagated to the periphery of the SAN and into the atrial muscle. From the atrial muscle, it propagated along the parallel slow and fast pathways into the AVN. Conduction along the fast pathway was faster than conduction along the slow pathway and as a result the action potential first entered the string of NH cells (penetrating bundle) via the fast pathway. Fig. 4 *D* is taken from De Carvalho et al. (14) and shows activation times (in ms) for the right atrium of the rabbit. The solid red or gray line roughly corresponds to the multicellular model and *a* to *e* in red roughly correspond to the center of the SAN (point *a*), periphery of the SAN (point *b*), atrial muscle at the starting point of the fast and slow pathways (point *c*), proximal penetrating bundle (point *d*), and bundle of His (point *e*). Comparison of Fig. 4, *C* and *D*, show that the action potential, having been initiated in the center of the SAN (point *a*), reached the periphery of the SAN (point *b*) in 37.5 ms in the experiment and 36 ms in the simulation, the atrial muscle at the starting point of the fast and slow pathways (point *c*) in 44 ms in the experiment and 47 ms in the simulation, the proximal penetrating bundle (point *d*) in 100 ms in the experiment and 99 ms in the simulation, and the bundle of His (point *e*) in 140 ms in the experiment and 129 ms in the simulation. Therefore, the simulation data are roughly in accord with the experimental data. In the model, if atrial cells are assumed to be 100 μm in length and arranged in parallel with the conduction pathway, the length of the atrial pathway is 7.5 mm and the conduction velocity of the atrial muscle is 69 cm/s. This compares favorably with experimentally measured values from the rabbit (~9–10 mm, M. R. Boyett, unpublished data, and 80 ± 29 cm/s (15)). If the N cells making up the slow pathway are assumed to be 100 μm in length and 10 μm in width, and arranged either in parallel with or transverse to the conduction pathway, the length of

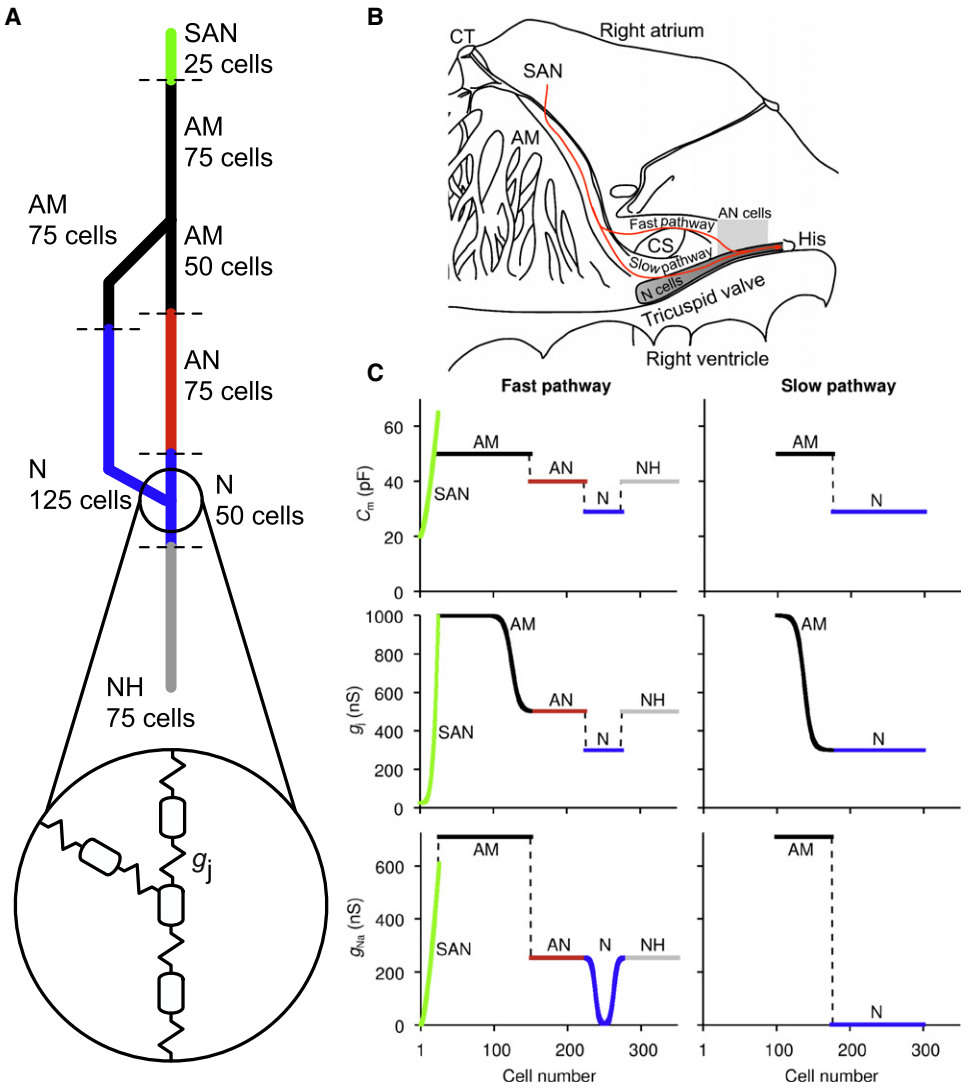

FIGURE 3 1D multicellular model including SAN, atrium, and AVN. (*A*) Schematic diagram of multicellular model. Multicellular model was composed of i), 25 SAN cells (*green* in PDF version); ii), 75 atrial cells (*black*); iii), 50 atrial (*black*), 75 AN (*red* in PDF version), and 25 N (*blue* in PDF version) cells making up fast pathway; iv), 75 atrial (*black*) and 125 N (*blue* in PDF version) cells making up slow pathway; and v), 25 N cells (*blue* in PDF version) and 75 NH cells (*gray*) making up penetrating bundle. Circled inset shows how neighboring cells were electrically coupled by coupling conductance, g_j. (*B*) Relationship between multicellular model (*red* or *gray line*) and rabbit right atrium. (*C*) Cell capacitance (C_m), coupling conductance (g_j), and Na^+ conductance (g_{Na}) along length of multicellular model. In PDF version, colors correspond to colors in *A*. AM, atrial muscle; CS, coronary sinus; CT, crista terminalis; His, bundle of His.

the slow pathway is either 12.5 or 1.25 mm and the conduction velocity of the slow pathway is either 17.1 or 1.71 cm/s; in the rabbit, the slow pathway is ~6–7 mm in length (M. R. Boyett, unpublished data) and the conduction velocity of the slow pathway is reported to be from 2 to 10 cm/s (16).

AV nodal reentry and effect of slow pathway ablation and $I_{Ca,L}$ block

To simulate AV nodal reentry, we used a S1-S2 protocol. Fig. 5 *A* shows the 1D multicellular model used. The configuration of the model (Fig. 5 *A*) is different to that of the model shown in Fig. 3 *A* (slow and fast pathways are shorter), but it is not unreasonable that the length of the pathways varies in different animals. Fig. 5 *B* shows a representative result. Selected action potentials are shown at the top left, more action potentials along the conduction pathway are shown at the top right, and activation times for the S1 and S2 action potentials are shown at the bottom. The atrial muscle was stimulated. In response to S1 stimulation (basic beat), the action potential propagated from the atrial muscle to the His bundle via the fast pathway of the AVN as described above. In response to S2 stimulation (premature beat; S1-S2 interval, 115 ms), the action potential again propagated along the string of atrial cells; it also propagated along the slow pathway (albeit more slowly). However, it failed to propagate along the fast pathway, because the fast pathway was refractory (refractory period of AN cells making up fast pathway is longer than refractory period of both atrial cells and N cells making up slow pathway; Table 1). By the time the action potential had propagated along the slow pathway, the fast pathway had become reexcitable and the action potential, as well propagating along the string of NH cells, propagated retrogradely along the fast pathway. This ultimately resulted in another atrial excitation as well as anterograde propagation along the slow pathway, i.e., AV nodal reentry. When the S1-S2 interval was longer than 124 ms, AV nodal reentry did not occur (conduction occurred normally) and, when the S1-S2 interval was between 111 and 115 ms, AV nodal reentry occurred. When

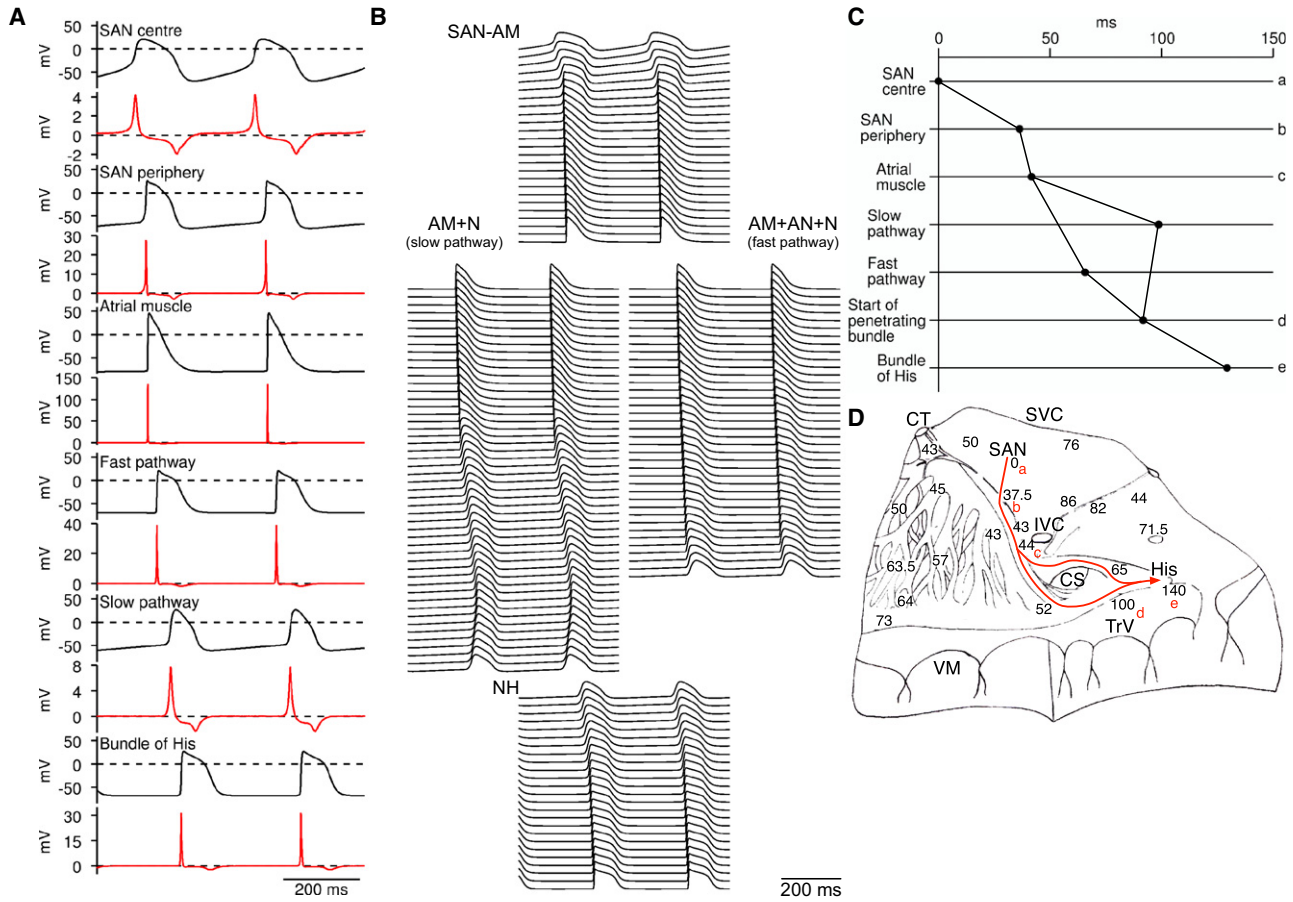

FIGURE 4 Action potential propagation from SAN to AVN. (*A*) Simulated action potentials and first derivative of membrane potential from center and periphery of SAN, atrial muscle, and AN, N, and NH cells. (*B*) Action potentials from many cells along length of 1D multicellular model. Action potentials from consecutive cells are displaced downward. (*C*) Activation times at the center and periphery of SAN, atrial muscle at start of fast and slow pathways into AVN, middle of fast and slow pathways, start of penetrating bundle, and bundle of His (middle of penetrating bundle). (*D*) Activation times (in ms) recorded experimentally in rabbit right atrial preparation including SAN and AVN during sinus rhythm (from De Carvalho et al. (14)). Red or gray line is approximately equivalent to multicellular model. Letters *a* to *e* identify points along conduction pathway from SAN to AVN at which activation time was measured in simulation: *a*, center of SAN; *b*, periphery of SAN; *c*, atrial muscle at start of fast and slow pathways into AVN; *d*, start of penetrating bundle; *e*, bundle of His. AM, atrial muscle; CS, coronary sinus; CT, crista terminalis; His, bundle of His; IVC, inferior vena cava; SVC, superior vena cava; TrV, tricuspid valve; VM, ventricular muscle.

the S1-S2 interval was shorter than 110 ms, action potential conduction through the AVN was blocked completely (Fig. 5 *C*); this corresponds to the refractory period of the slow pathway.

Clinically, AV nodal reentry is abolished by either the ablation of the slow pathway at the isthmus between the ostium of the coronary sinus and the tricuspid valve or by the application of a Ca^{2+} antagonist (17). In the model, both slow pathway ablation and 20% inhibition of the L-type Ca^{2+} current also abolished it (data not shown).

AVN conduction curve and effect of slow and fast pathway ablation

Fig. 6 *A* shows conduction curves, i.e., the relationship between the conduction time through the AVN (from atrial muscle to His bundle or final NH cell in simulations) and the S1-S2 interval from both simulation and experiment. The simulation data were obtained with the 1D multicellular model shown in Fig. 5 *A*. The simulation and experimental data are qualitatively similar: in both simulation and experiment, the conduction time was prolonged at short S1-S2 intervals and at the refractory period (of slow pathway) conduction failed (Fig. 6 *A*). In both simulation and experiment, slow pathway ablation lengthened the apparent refractory period and the initial limb of the conduction curve was lost – the remainder of the conduction curve was unaffected (Fig. 6 *B*). This shows that the slow pathway (with shorter refractory period than fast pathway) is responsible for the initial limb of the conduction curve, whereas the fast pathway is responsible for the remainder (Fig. 6 *B*). After fast pathway ablation, the slow pathway alone was responsible for the conduction curve. In both simulation and experiment, after fast pathway ablation, conduction was slowed at

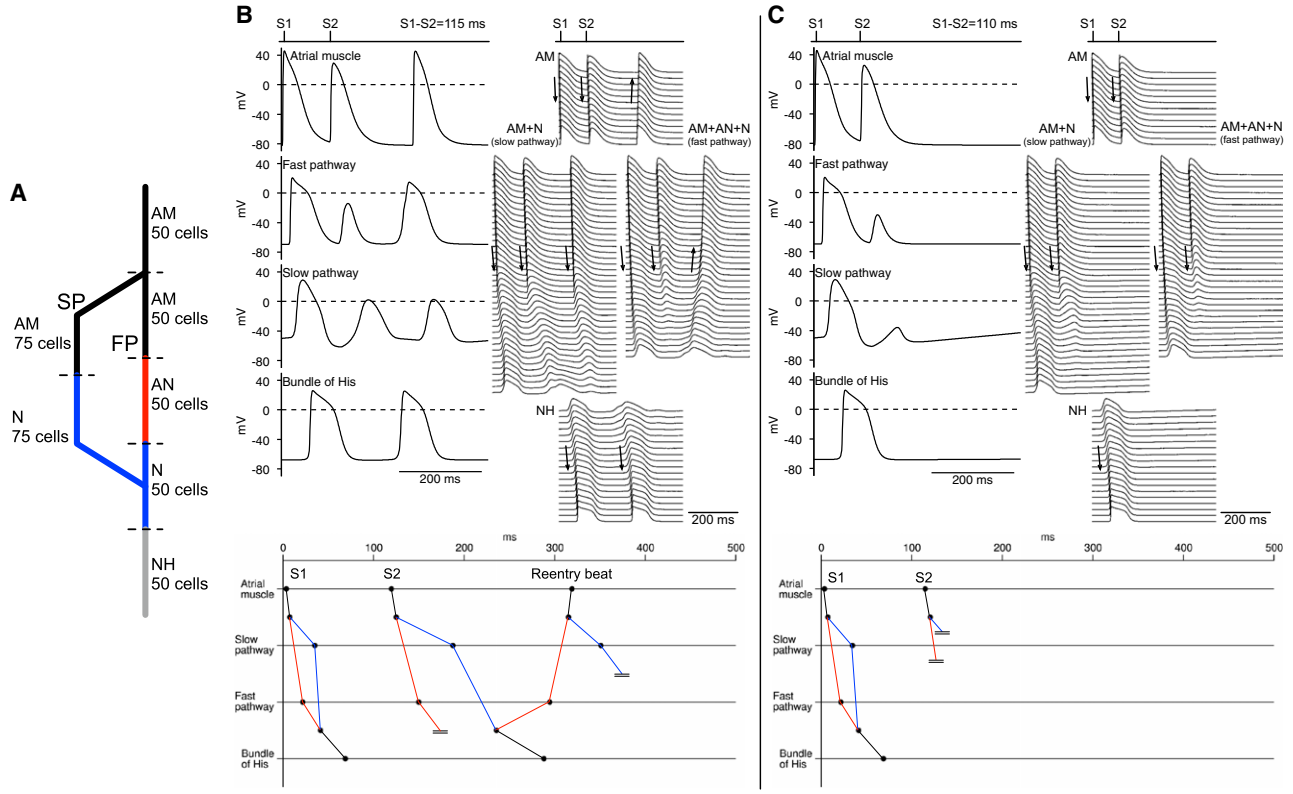

FIGURE 5 Simulated AV nodal reentry induced by S1-S2 protocol. (*A*) Schematic diagram of 1D multicellular model used. Multicellular model was composed of i), 50 atrial cells (*black*); ii), 50 atrial (*black*), 50 AN (*red* in PDF version) cells, and 25 N cells making up fast pathway; iii), 75 atrial (*black*) and 75 N (*blue* in PDF version) cells making up slow pathway; and iv), 25 N cells (*blue* in PDF version) and 50 NH cells (*gray*) making up penetrating bundle. (*B*) Reentry after S1-S2 interval of 115 ms. (*Top left*) Selected action potentials; (*Top right*), action potentials from many cells along length of multicellular model; bottom, activation times at middle of atrial muscle, middle of fast and slow pathways, and bundle of His (middle of penetrating bundle); conduction block is indicated by a pair of parallel lines. S1 and S2 beats were followed by reentry beat. (*C*) Conduction block after S1-S2 interval of 110 ms. Layout of *C* is same as that of *B*.

all S1-S2 intervals except the shortest, i.e., the conduction curve was pivoted upward at this point (Fig. 6 *C*).

Protecting ventricles during AF

During AF, the AVN protects the ventricles from high frequency excitation and this effect was investigated using the 1D multicellular model shown in Fig. 3 *A*. To simulate AF, the middle of the string of atrial cells was stimulated and the stimulus interval was randomly changed from 75 to 150 ms (18). Fig. 7 *A* shows action potentials at selected points (center and periphery of SAN, middle of atrial muscle, middle of fast and slow pathways, and middle of penetrating bundle) and Fig. 7 *B* shows the activation time at the same points. During AF, activity within the slow and fast pathways was irregular and frequent local conduction block occurred (local conduction block also occurred at SAN; Fig. 7 *A*). Consequently, the average frequency of action potentials reaching the bundle of His and the center of the SAN was reduced from 7.3 to 3.8 and 6.7 Hz, respectively; the activity of the bundle of His and the center of the SAN was also irregular.

Effect of $I_{Ca,L}$ block and AVN pacemaking

Block of $I_{Ca,L}$ is known to block conduction through the AVN (19). From simulations, Fig. 8 *A* shows atrial muscle, AN, N and NH action potentials under control conditions and after 30% block of $I_{Ca,L}$. After block of $I_{Ca,L}$, the action potential failed to conduct to the distal site. Fig. 8 *B* shows comparable data recorded from the rabbit AVN (19). In the rabbit, in the absence of stimulation, the AVN shows pacemaking and the pacemaker activity originates in the inferior nodal extension (slow pathway) (20). Fig. 9 shows that in the multicellular model, in the absence of stimulation, pacemaker activity originated in the N cells making up the slow pathway and it then propagated to the other tissues in this same way as in experiments.

DISCUSSION

Achievements of model

In this study, on the basis of experimental data, we have developed a family of single cell action potential models

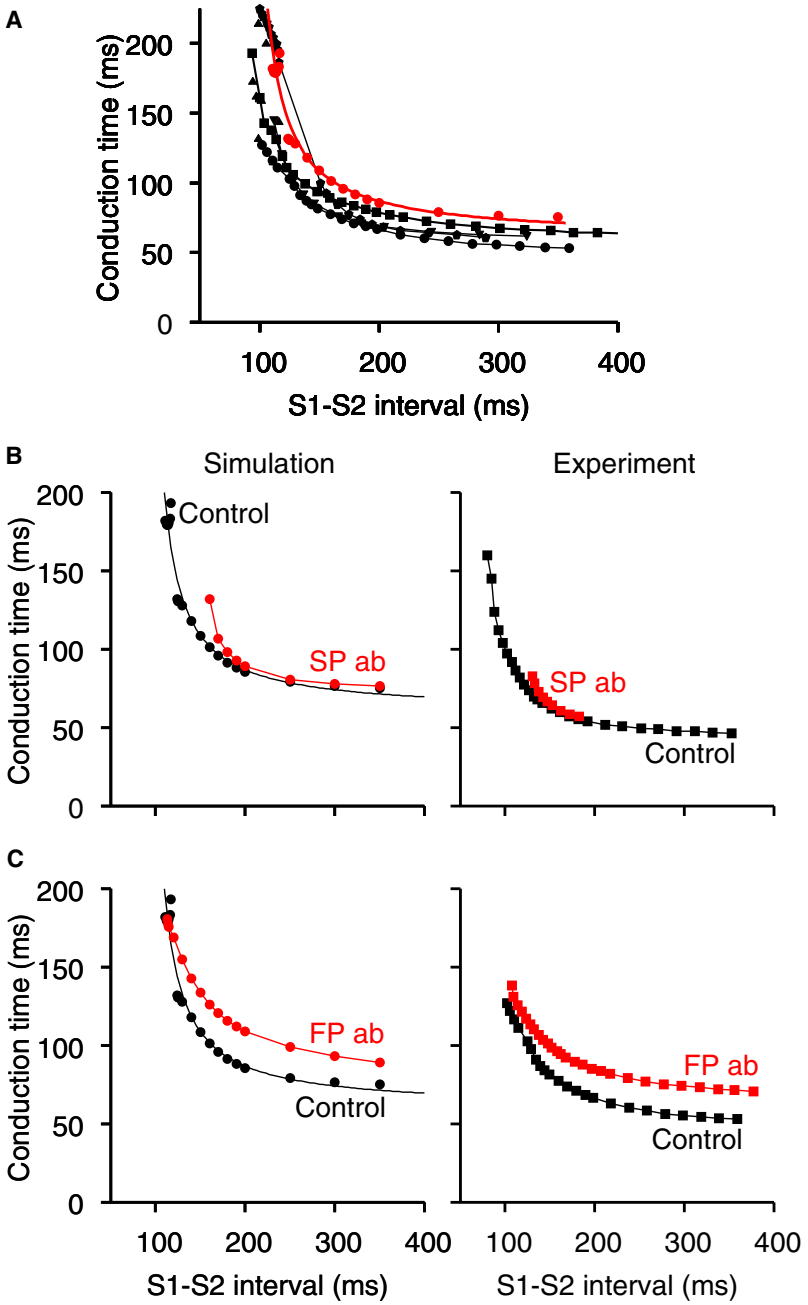

FIGURE 6 AVN conduction curves from simulation and experiment. (*A*) Conduction curves under control conditions from simulation (*red* or *gray*; 1D multicellular model in Fig. 5 *A* used) and experiment (*black*; rabbit AVN; *circles* (25); *triangles* (22); *inverted triangles* (9); *squares* (10); *pentagons* (43)). (*B*) Conduction curves under control conditions (*black*) and after slow pathway ablation (SP ab; *red* or *gray*) from simulation (*left*) and experiment (*right*; rabbit AVN (25)). (*C*) Conduction curves under control conditions (*black*) and after fast pathway ablation (FP ab; *red* or *gray*) from simulation (*left*) and experiment (*right*; rabbit AVN (25)).

for the AVN; the model action potentials are comparable to action potentials recorded from the rabbit AVN (Figs. 1 and 2). In addition, we have developed a 1D multicellular model including the SAN, atrial muscle, and AVN, and analyzed AVN characteristics such as its dual pathway electrophysiology. The multicellular model qualitatively replicates the behavior of the AVN and it is, therefore, a useful tool to analyze the characteristics of the AVN. The achievements of the multicellular model will be considered.

Slow conduction in the AVN

Under normal conditions, in all species including human, the AVN is responsible for slow conduction between the atria and the ventricles, and the fast pathway plays a major role in AVN conduction (21). In the multicellular model shown in Fig. 5 *A*, the conduction time from the atrial muscle to the His bundle was 75 ms, which is roughly consistent with experimental recordings from the rabbit AVN (10,16,22). Slow conduction through the AVN is presumed to be related to a low Na^+ conductance (g_{Na} (23)) and poor electrical coupling (i.e., low g_j) in the AVN and these factors were important in our model (Fig. 3 *C*).

Conduction curve

When a premature stimulus is applied at a short coupling interval, because of the difference in refractoriness between

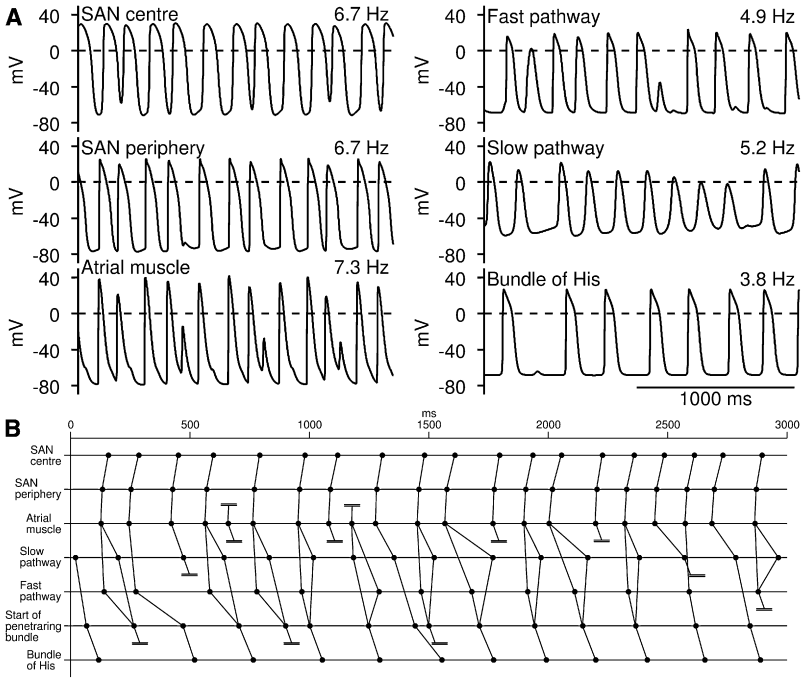

FIGURE 7 Protecting ventricles during atrial fibrillation. In this simulation, 1D multicellular model shown in Fig. 3 *A* was used. To simulate AF, middle of string of atrial cells was stimulated and stimulus interval was changed randomly from 75 to 150 ms. (*A*) Selected action potentials. (*B*) Activation times at center and periphery of SAN, middle of atrial muscle, middle of fast and slow pathways, start of penetrating bundle, and bundle of His (middle of penetrating bundle). Conduction block is indicated by pair of parallel lines.

the slow and fast pathways, action potential propagation switches from the fast pathway to the slow pathway. In this way, the slow pathway normally contributes to conduction only at short coupling intervals (24). Consistent with this, in our multicellular model, conduction occurred through the fast pathway at long and intermediate coupling intervals and through the slow pathway at short coupling intervals (Fig. 5 *B*); when the fast pathway failed to conduct, the slow pathway took over and accounted for the steep rising portion of the conduction curve (Fig. 6).

Reentry

After premature stimulation, if fast pathway conduction was blocked, then the action potential could propagate retrogradely along the fast pathway (after slow pathway conduction) to produce an atrial echo beat (Fig. 5 *B*). This scenario could also lead to reentry (Fig. 5 *B*). This behavior depends critically on differences in refractory periods. Table 1 compares refractory periods in simulations and experiment. Experimentally, refractory periods have been measured in whole AVN preparations (25,26). The refractory period of the intact AVN is assumed to represent the refractory period of the slow pathway, and the refractory period after slow pathway ablation is assumed to represent the refractory period of the fast pathway (assumptions supported by simulation data in Fig. 6). In simulations, refractory periods were similar to experimental values (Table 1). Reentry is also expected to depend on the reentry path length and the conduction velocity and this is true in this case. In the model shown in Fig. 3 *A* (with relatively long fast and slow pathways), reentry occurred at S1-S2 intervals between 110 and 122 ms (time window of 12 ms). However, in the model shown in Fig. 5 *A* (with relatively short fast and slow pathways), the time window was only 4 ms. The conduction velocity depends on the coupling conductance (g_j) and as expected reentry was sensitive to the coupling conductance. For example, in the model shown in Fig. 5 *A*, the time window was 7, 4 (normal value), and 0 ms when g_j in the slow pathway (between the N cells in the fast and slow pathways and penetrating bundle) was 300, 500 (normal value), and 700 nS.

Slow pathway ablation

In experiments on the rabbit, slow pathway ablation prolongs the refractory period and prevents conduction at short cycle lengths; slow pathway ablation also curtails the steep portion of the conduction curve, but leaves its baseline unchanged (25). In patients, slow pathway ablation is used to stop AV nodal reentrant tachycardia (27). In our multicellular model, slow pathway ablation also prolonged the refractory period, prevented conduction at short cycle lengths, altered the conduction curve, and abolished reentry (Fig. 6; data not shown).

AVN filtering

Slow AV conduction is important during AF by limiting the number of action potentials transmitted to the ventricles (21). Using our multicellular model, we could simulate the AVN filtering function. Because the refractory period of the AVN is longer than that of the atrial muscle (Table 1), only a fraction of the atrial action potentials were transmitted to the ventricles during AF (Fig. 7).

Ca^{2+} channel block

Ca^{2+} channel antagonists are effective in ventricular rate control in patients with AF (28) and in controlling AV nodal reentrant tachycardia (29). In our multicellular model, in

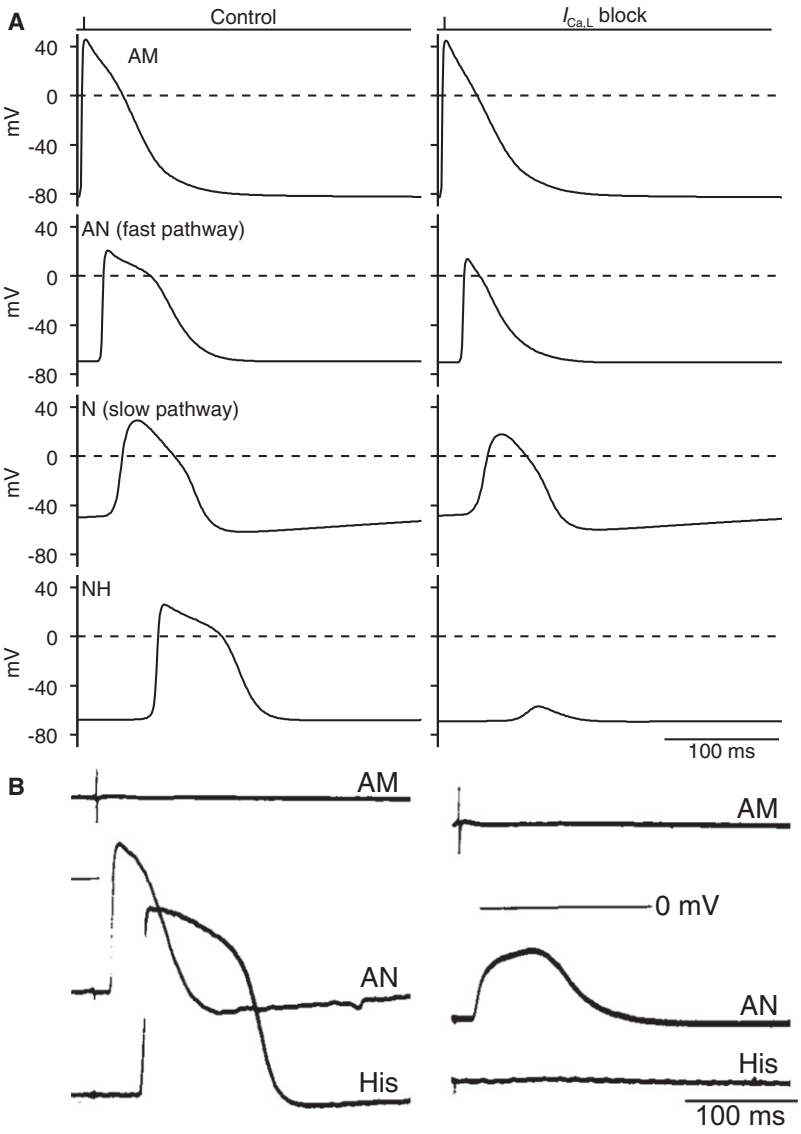

FIGURE 8 Comparison of effect of block of $I_{Ca,L}$ in simulation and experiment. (*A*) Selected simulated action potentials from atrial, AN, N and NH cells along length of 1D multicellular model (multicellular model shown in Fig. 5 *A* was used) under control conditions (*left*) and after 30% block of $I_{Ca,L}$ in all cells (*right*). (*B*) Equivalent experimental recordings of action potentials from rabbit AVN under control conditions (*left*) and after block of $I_{Ca,L}$ by 4 mM $MgCl_2$ (*right*) from Zipes and Mendez (19). Recording of extracellular potential from atrial muscle as well as intracellular recordings of membrane potential from AN and His cells are shown. Under control conditions, action potential propagated through AVN in both simulation and experiment. After block of $I_{Ca,L}$, AV block occurred in both simulation and experiment. AM, atrial muscle; His, bundle of His.

simulations of AF (Fig. 7), when the L-type Ca^{2+} current was decreased by 25%, ventricular rate was decreased from ~4.3 to ~2.6 Hz (data not shown), and when the L-type Ca^{2+} current was decreased by 20%, AV nodal reentry did not occur after premature stimulation (data not shown).

AVN pacemaking

It is well known that when the SAN fails, the AVN can take over as the pacemaker and, in the rabbit, it is the inferior nodal extension (slow pathway) that is the leading pacemaker site (30). This was also true with our multicellular model (Fig. 9). In the multicellular model, the spontaneous cycle length was 350 ms when the SAN was the pacemaker (Fig. 4) and 532 ms when the AVN was the pacemaker (Fig. 9). In comparison, in experiments on the rabbit, the spontaneous cycle length was 348 ± 50 ms in the case of the SAN (31) and 611 ± 84 ms in the case of the AVN (20).

Model limitations

Although the models developed in this study are a significant improvement on earlier models (4), they have limitations. For example, the electrophysiological data for the rabbit AVN are incomplete (e.g., there are no experimental data for kinetics of I_{Na}) and there is variability in the experimental data (e.g., in action potential parameters and ionic current densities). We have developed models of three cell types (AN, N, and NH). Billette (9), however, has also described ANL, ANCO, and H cells at the rabbit AV junction. Furthermore, the 1D multicellular model of the AVN presented in this study ignores the complexities of the structure of the AVN. For example, Hucker et al. (32) have shown the existence of two domains, with different conduction properties and gene expression, within the compact node in the rabbit and human. However, we have developed an anatomically detailed 3D model of the rabbit AVN and in preliminary

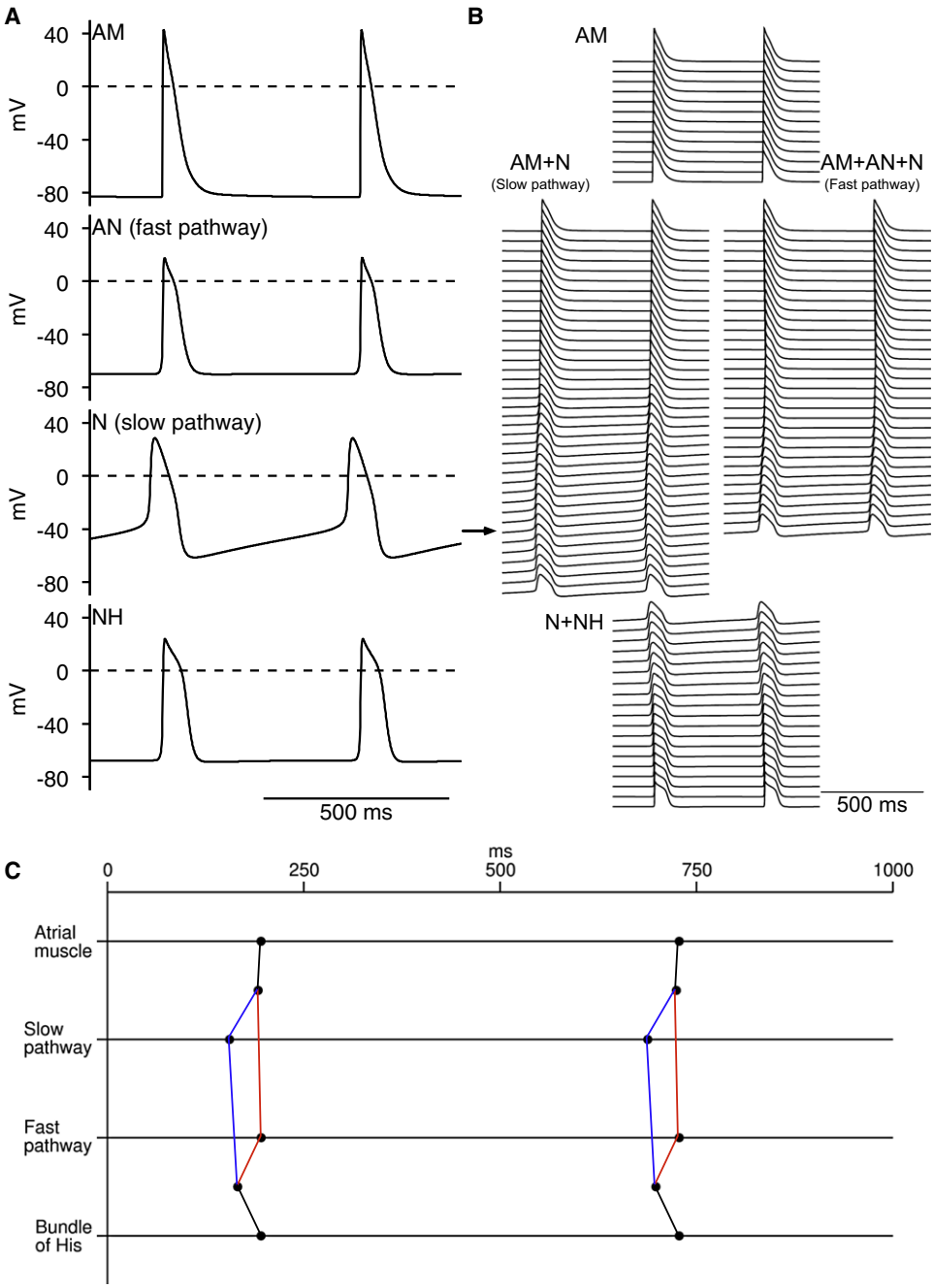

FIGURE 9 Pacemaker activity in 1D multicellular model of AVN. Multicellular model shown in Fig. 5 *A* was used; it did not include SAN. (*A*) Selected action potentials. (*B*) Action potentials from many cells along length of multicellular model. (*C*) Activation times at middle of atrial muscle, middle of fast and slow pathways and bundle of His (middle of penetrating bundle). In absence of stimulation, AVN acted as pacemaker. Horizontal arrow in *B* indicates leading pacemaker site in slow pathway. Action potential propagated from leading pacemaker site in slow pathway to atrial muscle and NH cells; in addition, action potential propagated to center of fast pathway from both ends of fast pathway. AM, atrial muscle.

simulations we combined this with the action potential models described in this study to compute normal AV conduction as well as AV nodal reentry (33,34).

CONCLUSIONS

In this study, we have developed action potential models for the rabbit AVN. Action potential models for other regions of the rabbit heart have already been developed (3). This brings a model of the whole heart (a virtual heart) with accurate electrophysiology and anatomy, an important research and teaching tool, one step nearer.

SUPPORTING MATERIAL

Methods, references, seven figures, and 18 tables are available at http://www.biophysj.org/biophysj/supplemental/S0006-3495(09)01353-8.

This work was supported by the British Heart Foundation (RG/06/005) and the Biotechnology and Biological Sciences Research Council (BBS/B/1678X).

REFERENCES

1. Meijler, F. L., and M. J. Janse. 1988. Morphology and electrophysiology of the mammalian atrioventricular node. *Physiol. Rev.* 68:608–647.

2. Petrecca, K., and A. Shrier. 2000. Spatial distribution of ion channels, receptors, and innervation. *In* Atrial-AV Nodal Electrophysiology: A View from the Millennium. T. N. Mazgalev and P. J. Tchou, editors. Futura Publishing, New York. 89–105.
3. Boyett, M. R., J. Li, S. Inada, H. Dobrzynski, J. E. Schneider, et al. 2005. Imaging the heart: computer 3-dimensional anatomic models of the heart. *J. Electrocardiol.* 38:113–120.
4. Liu, Y., W. Zeng, M. Delmar, and J. Jalife. 1993. Ionic mechanisms of electronic inhibition and concealed conduction in rabbit atrioventricular nodal myocytes. *Circulation.* 88:1634–1646.
5. Hancox, J. C., K. H. Yuill, J. S. Mitcheson, and M. K. Convery. 2003. Progress and gaps in understanding the electrophysiological properties of morphologically normal cells from the cardiac atrioventricular node. *Int. J. Bifurcat. Chaos.* 13:3675–3691.
6. de Carvalho, A., and D. de Almeida. 1960. Spread of activity through the atrioventricular node. *Circ. Res.* 8:801–809.
7. Munk, A. A., R. A. Adjemian, J. Zhao, A. Ogbaghebriel, and A. Shrier. 1996. Electrophysiological properties of morphologically distinct cells isolated from the rabbit atrioventricular node. *J. Physiol.* 493:801–818.
8. Ren, F. X., X. L. Niu, Y. Ou, Z. H. Han, F. D. Ling, et al. 2006. Morphological and electrophysiological properties of single myocardial cells from Koch triangle of rabbit heart. *Chin. Med. J.* 119:2075–2084.
9. Billette, J. 1987. Atrioventricular nodal activation during periodic premature stimulation of the atrium. *Am. J. Physiol.* 252:H163–H177.
10. Medkour, D., A. E. Becker, K. Khalife, and J. Billette. 1998. Anatomic and functional characteristics of a slow posterior AV nodal pathway: role in dual-pathway physiology and reentry. *Circulation.* 98:164–174.
11. Greener, I. D., J. Tellez, H. Dobrzynski, M. Yamamoto, G. M. Graham, et al. 2009. Ion channel transcript expression at the rabbit atrioventricular conduction axis. *Circ. Arrhythmia Electrophysiol.* 2:305–315.
12. Zhang, H., A. V. Holden, I. Kodama, H. Honjo, M. Lei, et al. 2000. Mathematical models of action potentials in the periphery and center of the rabbit sinoatrial node. *Am. J. Physiol.* 279:H397–H421.
13. Lindblad, D. S., C. R. Murphey, J. W. Clark, and W. R. Giles. 1996. A model of the action potential and underlying membrane currents in a rabbit atrial cell. *Am. J. Physiol.* 271:H1666–H1696.
14. de Carvalho, A. P., W. C. Mello, and B. F. Hoffman. 1959. Electrophysiological evidence for specialized fiber types in rabbit atrium. *Am. J. Physiol.* 196:483–488.
15. de Groot, J. R., T. Veenstra, A. O. Verkerk, R. Wilders, J. P. Smits, et al. 2003. Conduction slowing by the gap junctional uncoupler carbenoxolone. *Cardiovasc. Res.* 60:288–297.
16. Efimov, I. R., V. P. Nikolski, F. Rothenberg, I. D. Greener, J. Li, et al. 2004. Structure-function relationship in the AV junction. *Anat. Rec.* 280:952–965.
17. Goy, J. J., and M. Fromer. 1991. Antiarrhythmic treatment of atrioventricular tachycardias. *J. Cardiovasc. Pharmacol.* 17 (Suppl):S36–S40.
18. Mazgalev, T. N., S. Garrigue, K. A. Mowrey, Y. Yamanouchi, and P. J. Tchou. 1999. Autonomic modification of the atrioventricular node during atrial fibrillation: role in the slowing of ventricular rate. *Circulation.* 99:2806–2814.
19. Zipes, D. P., and C. Mendez. 1973. Action of manganese ions and tetrodotoxin on atrioventricular nodal transmembrane potentials in isolated rabbit hearts. *Circ. Res.* 32:447–454.
20. Dobrzynski, H., V. P. Nikolski, A. T. Sambelashvili, I. D. Greener, M. Yamamoto, et al. 2003. Site of origin and molecular substrate of atrioventricular junctional rhythm in the rabbit heart. *Circ. Res.* 93:1102–1110.
21. Zhang, Y., and T. N. Mazgalev. 2004. Ventricular rate control during atrial fibrillation and AV node modifications: past, present, and future. *Pacing Clin. Electrophysiol.* 27:382–393.
22. Nikolski, V. P., S. A. Jones, M. K. Lancaster, M. R. Boyett, and I. R. Efimov. 2003. Cx43 and dual-pathway electrophysiology of the atrioventricular node and atrioventricular nodal reentry. *Circ. Res.* 92:469–475.
23. Kleber, A. G., and Y. Rudy. 2004. Basic mechanisms of cardiac impulse propagation and associated arrhythmias. *Physiol. Rev.* 84:431–488.
24. Patterson, E., and B. J. Scherlag. 2002. Anatomic and functional fast atrioventricular conduction pathway. *J. Cardiovasc. Electrophysiol.* 13:945–949.
25. Reid, M. C., J. Billette, K. Khalife, and R. Tadros. 2003. Role of compact node and posterior extension in direction-dependent changes in atrioventricular nodal function in rabbit. *J. Cardiovasc. Electrophysiol.* 14:1342–1350.
26. Lin, L. J., J. Billette, D. Medkour, M. C. Reid, M. Tremblay, et al. 2001. Properties and substrate of slow pathway exposed with a compact node targeted fast pathway ablation in rabbit atrioventricular node. *J. Cardiovasc. Electrophysiol.* 12:479–486.
27. Haissaguerre, M., F. Gaita, B. Fischer, D. Commenges, P. Montserrat, et al. 1992. Elimination of atrioventricular nodal reentrant tachycardia using discrete slow potentials to guide application of radiofrequency energy. *Circulation.* 85:2162–2175.
28. Lundstrom, T., and L. Ryden. 1990. Ventricular rate control and exercise performance in chronic atrial fibrillation: effects of diltiazem and verapamil. *J. Am. Coll. Cardiol.* 16:86–90.
29. Philippon, F., V. J. Plumb, and G. N. Kay. 1994. Differential effect of esmolol on the fast and slow AV nodal pathways in patients with AV nodal reentrant tachycardia. *J. Cardiovasc. Electrophysiol.* 5:810–817.
30. Watanabe, Y., and L. S. Dreifus. 1968. Sites of impulse formation within the atrioventricular junction of the rabbit. *Circ. Res.* 22:717–727.
31. Kirchhof, C. J., F. I. Bonke, M. A. Allessie, and W. J. Lammers. 1987. The influence of the atrial myocardium on impulse formation in the rabbit sinus node. *Pflugers Arch.* 410:198–203.
32. Hucker, W. J., M. L. McCain, J. I. Laughner, P. A. Iaizzo, and I. R. Efimov. 2008. Connexin 43 expression delineates two discrete pathways in the human atrioventricular junction. *Anat. Rec. (Hoboken).* 291: 204–215.
33. Li, J., I. D. Greener, S. Inada, V. P. Nikolski, M. Yamamoto, et al. 2008. Computer three-dimensional reconstruction of the atrioventricular node. *Circ. Res.* 102:975–985.
34. Inada, S., J. Li, H. Dobrzynski, I. Greener, J. Hancox, et al. 2008. Simulation of atrioventricular nodal reentry using detailed anatomical and action potential models. Physiological Society Main Meeting Abstracts. 86P.
35. Mitcheson, J. S., and J. C. Hancox. 1999. Characteristics of a transient outward current (sensitive to 4-aminopyridine) in Ca^{2+}-tolerant myocytes isolated from the rabbit atrioventricular node. *Pflugers Arch.* 438:68–78.
36. Ruiz-Ceretti, E., and A. P. Zumino. 1976. Action potential changes under varied $[Na^{+}]_o$ and $[Ca^{2+}]_o$ indicating the existence of two inward currents in cells of the rabbit atrioventricular node. *Circ. Res.* 39: 326–336.
37. Akiyama, T., and H. A. Fozzard. 1979. Ca and Na selectivity of the active membrane of rabbit AV nodal cells. *Am. J. Physiol.* 236:C1–C8.
38. Nakayama, T., Y. Kurachi, A. Noma, and H. Irisawa. 1984. Action potential and membrane currents of single pacemaker cells of the rabbit heart. *Pflugers Arch.* 402:248–257.
39. Hirata, A. 1990. Effect of hypoxia on electrical activity of atrioventricular nodal cells and atrial cells of the rabbit's heart. *J. Electrocardiol.* 23:69–76.
40. Hewett, K. W., C. H. Gaymes, C. I. Noh, B. A. Ross, R. P. Thompson, et al. 1991. Cellular electrophysiology of neonatal and adult rabbit atrioventricular node. *Am. J. Physiol.* 260:H1674–H1684.
41. Guo, J., and A. Noma. 1997. Existence of a low-threshold and sustained inward current in rabbit atrio-ventricular node cells. *Jpn. J. Physiol.* 47:355–359.
42. Yi, K. H., and H. S. Han. 2000. Cellular electrophysiology of fast pathway ablation of rabbit atrioventricular node. *J. Korean Med. Sci.* 15:494–500.
43. Mazgalev, T. N., and P. J. Tchou. 2000. Surface potentials from the region of the atrioventricular node and their relation to dual pathway electrophysiology. *Circulation.* 101:2110–2117.